Characterization of InN-In$_{0.25}$Ga$_{0.75}$N Quantum Well Laser Structure for 1330 nm Wavelength

Md. Mobarak Hossain Polash [a,b], and M. Shah Alam [a]

[a] Department of Electrical and Electronic Engineering,
Bangladesh University of Engineering & Technology (BUET), Dhaka-1000, Bangladesh

[b] Department of Electrical and Electronic Engineering,
University of Asia Pacific (UAP), Dhaka-1209, Bangladesh

A nitride based wurtzite-strained QW laser with 12Å InN well layer, 15Å In$_{0.25}$Ga$_{0.75}$N barrier layer and GaN SCH layer has been designed and characterized at 1330nm wavelength. To determine the electronic properties, a self-consistent method with 6-bands **k.p** formalism considering valence-band mixing effect, strain and polarization effect followed by Poisson's equation has been used. The interband momentum matrix elements, optical gain, spontaneous emission rate, and radiative current density have been calculated to analyze the optical properties of the laser. Due to the strain effect, the wave-function overlap integral was obtained as 43.27%. The structure is TE polarized with C1-HH1 and C1-LH1 dominating transitions, while the spontaneous emission rate per energy interval per unit volume was $7.21×10^{27}$ s^{-1}cm^{-3}eV^{-1} at 1329.55nm. Furthermore, the radiative recombination rate and the radiative current density were $7.77×10^{29}$ s^{-1}cm^{-3} and 149.19 Acm^{-2}, respectively. The optical gain of the structure is 5261.52cm^{-1} at 1336.7nm for TE-polarization.

Introduction

In the last decade, a lot of fundamental and applied research has been done on Nitride semiconductors for lasers and light-emitting diodes (LEDs) in the blue-green and ultraviolet spectral regions (1-4). As Nitride lasers and light-emitting diodes (LEDs) have higher lifetimes which make it more commercially attractive over previously used II-VI devices (5). Quite recently nitride based single or multiple quantum wells are also studied in the spectral range over 1100 nm due to the prospect of their applications in optoelectronic devices like waveguide switches, infrared photo-detectors etc. For modern optical communication, particularly the wavelengths of 1330 nm and 1550 nm are most important for short distance and long distance communication respectively. As at 1330 nm, dispersion of a signal is lowest when at 1550 nm path loss of a signal is the lowest. Dispersion in the 1300 nm band (1285-1330 nm) must be less than 3.5 ps/nm/km (Picoseconds of dispersion per nanometer of signal bandwidth per kilometer of distance travelled) (6). At wavelengths around 1550 nm dispersion should be less than 20 ps/nm/km. Bend loss (at 1550 nm) must be less than 1 dB for travel through 100 turns of fibre wound on a spool of 7.5 cm diameter (6). As a result, III-nitride semiconductors like GaN, AlN, InN and their alloys are attracting much interest for optoelectronic devices in near-infrared spectral range particularly in 1330 nm to 1550 nm wavelength range for

fiber optic telecommunications. At longer wavelengths above 1650 nm, ambient temperature becomes background noise, disturbing signals (7). For designing nitride based semiconductor lasers and LEDs in communication wavelength spectra, generally intersubband (ISB) optoelectronic devices are mostly studied due to the large conduction band offset of the III-nitride heterostructures (8). For this range, design of interband structures are hardly proposed in any recent published works. For attaining the wavelength range, InN is most suitable nitride materials which is mostly proposed as quantum well (QW) material of delta well along with InGaN QWs (9). In this paper, design and analysis have been performed for InN as quantum well material and InGaN as barrier material. Here, GaN has been used as separate confinement heterostructure (SCH). In QW diode laser, SCH is used for better optical confinement as well as carrier confinement in the active region (10). For the analysis, the calculation of the band structures and wave functions of the Laser structure has been performed by using a self-consistent model where Schrodinger equation has been solved with Poisson's equation. Schrodinger equation has been formed with the effective mass Hamiltonian for conduction band and six-band **k.p** method for valence band (11). In this work, a wurtzite-strained nitride QW laser has been designed and an analysis of optical properties including optical gain, spontaneous emission spectrum, radiative current density along with interband momentum matrix elements have been carried out after solving the electronic properties of the structure.

Numerical Model

<u>Calculation of Electronic Properties</u>

For the calculation of the electronic band structure of a nitride based material system, electron and hole wave functions are calculated based on 6-band **k.p** formalism for wurtzite semiconductors (11). The model takes into account the valence band mixing effect, strain effect due to the lattice mismatch of nitride materials, spontaneous and piezoelectric polarization effect. In this model, the coupling between the conduction and valence bands, many-body Coulomb effects, carrier screening effect and inhomogeneous broadening of In-content are neglected. In this model, Strain due to lattice mismatch which is created in heterostructures grown by modern epitaxial techniques, is incorporated into the calculation using the deformation potentials (12). In this work, a strained InN wurtzite layer pseudomorphically grown along the c axis (z axis) on an $In_xGa_{1-x}N$ wurtzite layer. In the formalism of conduction band Hamiltonian, the electron energy bands are assumed to be parabolic in nature. The Hamiltonian based on effective mass approximation can be written as (11)

$$H^c(k_t, k_z) = \frac{\hbar^2}{2} \left(\frac{k_t^2}{m_e^t} + \frac{k_z^2}{m_e^z} \right) + E_c^0(z) + P_{c\varepsilon}(z) \qquad [1]$$

where, the wave vector $k_t = -i\nabla_t$, $k_z = -i\partial / \partial z$ and m_e^t and m_e^z are the electron effective masses perpendicular (t) and parallel (z) to the growth direction respectively. The hydrostatic energy shift in the conduction band, $P_{c\varepsilon}(z)$ is zero in the barrier regions and nonzero in the well region due to a strain effect (11). The spontaneous polarization has been calculated by using linear interpolation scheme (13). Due to polarization, in wurtzite III-nitride semiconductors have a built-in internal electrostatic fields in each layer which leads to energy band bending (13). To ensure zero average electric field in the layers,

electric field needs to satisfy the periodic boundary conditions described in (13). The bulk valence-band structure can be determined by finding the eigenvalues of the Hamiltonian of the valence-band using 6×6 diagonalized ***k.p*** Hamiltonian matrix (11, 14)

$$H_{6\times6}{}^v(\text{k}) = \begin{bmatrix} H_{3\times3}{}^U(\text{k}) & 0 \\ 0 & H_{3\times3}{}^L(\text{k}) \end{bmatrix} \qquad [2]$$

where $H_{3\times3}{}^U$ and $H_{3\times3}{}^L$ are three by three matrices defined as (11, 14)

$$H^U = \begin{bmatrix} F & K_t & -iH_t \\ K_t & G & \Delta - iH_t \\ iH_t & \Delta + iH_t & \lambda \end{bmatrix} \qquad [3]$$

$$H^L = \begin{bmatrix} F & K_t & iH_t \\ K_t & G & \Delta + iH_t \\ -iH_t & \Delta - iH_t & \lambda \end{bmatrix} \qquad [4]$$

Here the reference energy, $E_v{}^0$ which should appear in all the diagonal terms of the matrices, has been set to zero for a bulk semiconductor. The matrix elements contain the general expressions for a strained wurtzite semiconductor (11, 14). The parameter value of nitride binary materials (GaN, InN and AlN) has been taken from (5, 14-15).

Formulation of Optical gain and Spontaneous Emission with Transition Matrix Elements

By using the obtained envelop functions, the optical interband transition (momentum) matrix elements relating nth-state in the conduction band and mth-state valence band are computed by the following relations (11, 14):

TE-polarization ($\hat{e} = \hat{x}$ or $\hat{y} \perp c$ axis):

$$\left|(M_x)_{nm}^{\sigma}(\text{k}_t)\right|^2 = \frac{\left|\langle S | p_x | X \rangle\right|^2}{4} \cdot \left\{ \left\langle \phi_n | g_m^{(1)} \right\rangle^2 + \left\langle \phi_n | g_m^{(2)} \right\rangle^2 \right\} \quad \text{for} \quad \sigma = U$$

$$= \frac{\left|\langle S | p_x | X \rangle\right|^2}{4} \cdot \left\{ \left\langle \phi_n | g_m^{(4)} \right\rangle^2 + \left\langle \phi_n | g_m^{(5)} \right\rangle^2 \right\} \quad \text{for} \quad \sigma = L. \qquad [5]$$

TM-polarization ($\hat{e} = \hat{z} \parallel c$ axis):

$$\left|(M_z)_{nm}^{\sigma}(\text{k}_t)\right|^2 = \frac{\left|\langle S | p_z | Z \rangle\right|^2}{2} \cdot \left\langle \phi_n | g_m^{(3)} \right\rangle^2 \quad \text{for} \quad \sigma = U$$

$$= \frac{\left|\langle S | p_z | Z \rangle\right|^2}{2} \cdot \left\langle \phi_n | g_m^{(6)} \right\rangle^2 \quad \text{for} \quad \sigma = L. \qquad [6]$$

where, ϕ_n and g_m are conduction and valence band confined states respectively. The upper and lower Hamiltonian blocks are indicated by $\sigma = U$ and $\sigma = L$ respectively. In our calculations here, the linewidth broadening time (τ_s) is assumed to have Lorentzian shape

with τ_s = 0.1 ps. The necessary values of different parameters are taken from (5, 14-15). Based on the Fermi's Golden rule, the spontaneous emission rate for TE ($e = x$) or TM ($e = z$) polarizations can be obtained by taking into account all interband transitions between nth conduction band and mth valence subbands as follows (11, 14):

$$g_{sp}^{e}(\hbar\omega) = \frac{2q^2\pi}{n_r c \varepsilon_0 m_0^2 \omega L_w} \sum_{\sigma=U,L} \sum_{n,m} \int \frac{k_t dk_t}{2\pi} |(M_e)_{nm}^{\sigma}(k_t)|^2 \frac{f_n^c(k_t)(1-f_{\sigma m}^v(k_t))(\gamma/\pi)}{(E_{\sigma,nm}^{cv}(k_t)-\hbar\omega)^2 + \gamma^2} \quad [7]$$

For the calculation of the spontaneous emission rate, both TE and TM polarizations are taken into account. The total momentum matrix element is the angular average of two TE-polarization components and one TM-polarization component (11). The total spontaneous emission rate per unit volume per unit energy interval ($s^{-1}cm^{-3}eV^{-1}$) can be written as fellows (11, 14):

$$r^{spon}(E = \hbar\omega) = \frac{n_e^2 \omega^2}{\pi^2 \hbar c^2} \frac{2(2g_{sp}^x + g_{sp}^z)}{3} \quad [8]$$

The total spontaneous emission rate per unit volume ($s^{-1}cm^{-3}$) is obtained by integrating equation [8] over entire frequency range as follows (14)

$$R_{sp} = \int_0^{\infty} r_{sp}(\hbar\omega) d(\hbar\omega) \quad [9]$$

Thus, the radiative recombination current density (A/cm^2) is defined as (14)

$$J_{rad} = qdR_{sp} \quad [10]$$

where, d is the active region length. In the calculations of the spontaneous emission spectra and optical gain, it is necessary to include all possible transitions between electron and hole confined states in the QW region, as the polarization field-induced band bending in the III-Nitride QW leads to the breaking of the orthogonality condition between states with different quantum numbers (16).

Design of the Laser Structure and Analysis of its Properties

In this work, 12Å InN quantum well layer has been sandwiched between two 15Å In$_{0.25}$Ga$_{0.75}$N barrier layers. At both end of the barrier layer, a separate confinement heterostructure of GaN has been used to provide the better optical and carrier confinement. Figure 1 shows the structure against z-axis (device growing length) indicating all regions with respective materials along with the energy band lineup for 1st conduction and 1st valence subband wavefunction. Energy band lineup in Figure 1 includes the effect of internal electric field due to polarization and strain effect. Here, the envelop functions of the electron-hole wavefunction has been depicted as a function of device length and the overlap integral between the wavefunction has been also illustrated. In our work, the obtained overlap integral factor is 43.27%. From figure, it can be inferred that the higher wavefunction overlap integral factor will cause higher radiative recombination hence higher optical output.
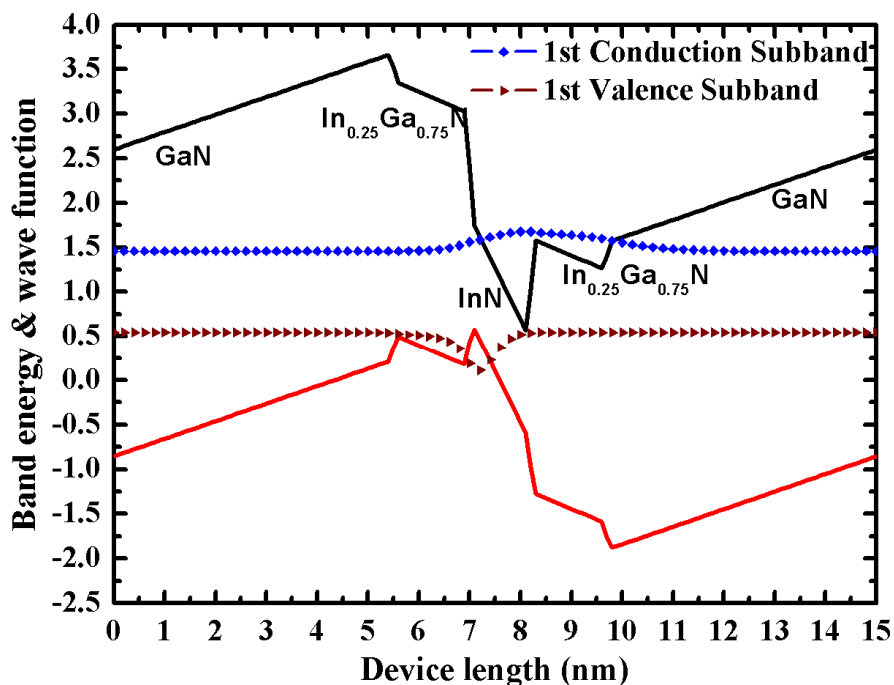
Figure 1. Energy band edge profile of conduction and valence band with internal electric field for InN (12Å)/ In$_{0.25}$Ga$_{0.75}$N (15Å) SQW Laser system sandwiched between GaN SCH region with electron and hole wave function.

In Figure 2(a) and 2(b), the conduction band structures (first 8 subbands) and the valence subband structures (first 8 subbands) have been shown as a function of the in-plane wavenumber k_t. HH (heavy-hole) and LH (light-hole) valence subbands are shown in Figure 2(b) depending on their nature. In this work, bowing parameter of InGaN for gamma energy band calculation is 1.4 eV and for spontaneous polarization calculation is -0.037C/m^2 (10).
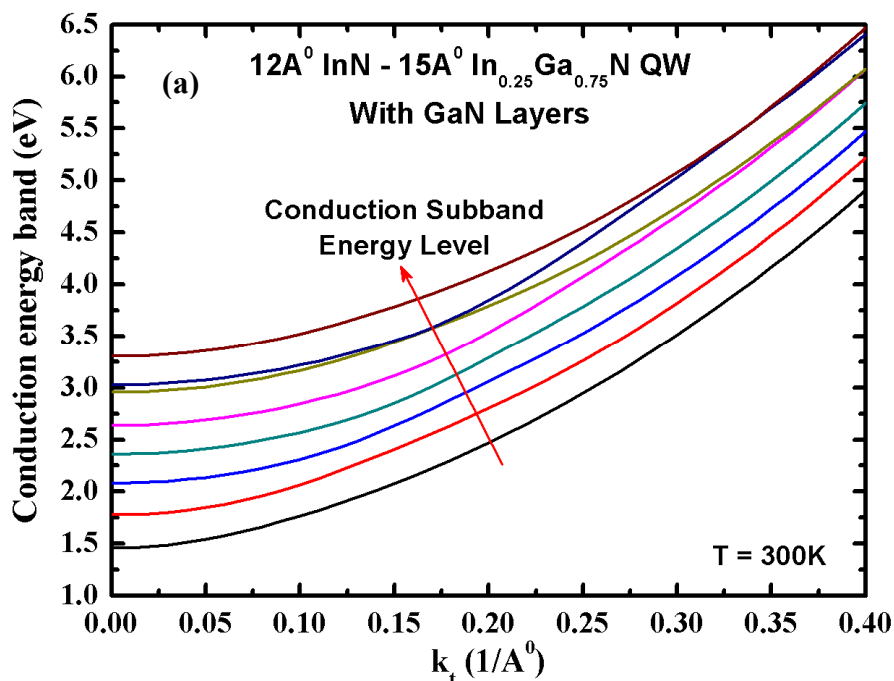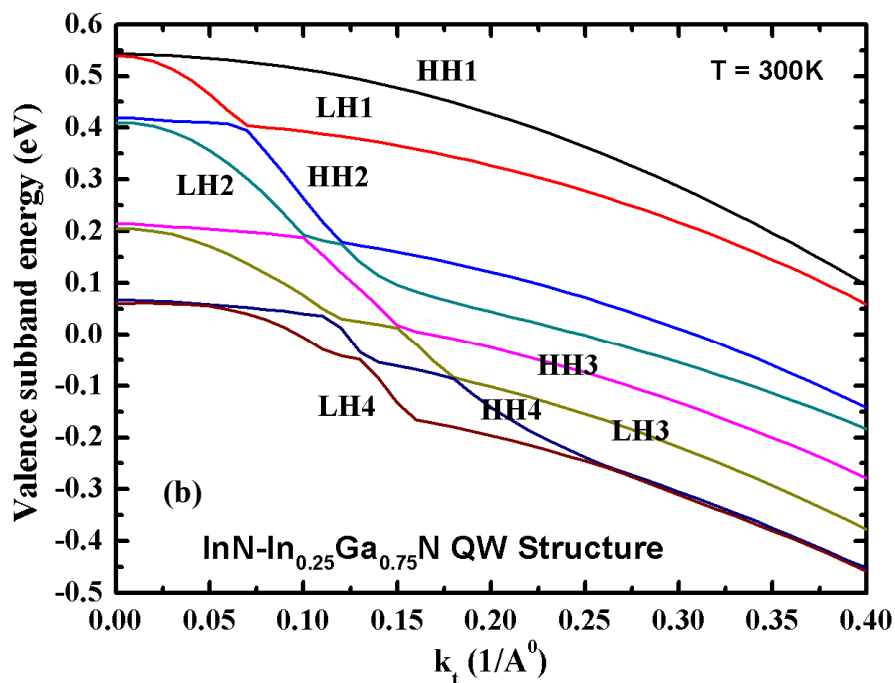
Figure 2. (a) Conduction energy subbands and (b) Valence energy subbands for 12Å InN / 15Å In$_{0.25}$Ga$_{0.75}$N SQW material system along with GaN SCH.

In Figure 3, four consecutive conduction wavefunctions have been shown along with their corresponding energy subband levels with respect to device length. In our designed structure, first energy level of conduction subband is found at 1.457 eV. The second, third and fourth conduction subband energy levels are 1.78 eV, 2.08 eV and 2.36 eV respectively.
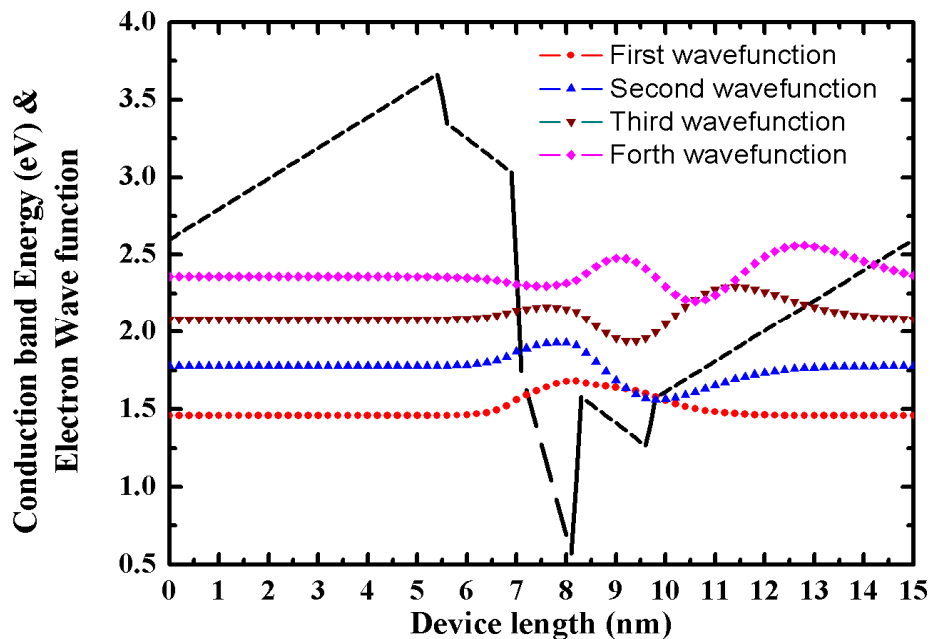

Figure 3. First four envelop functions of the laser system along the device length. Frist one is totally bound within active region when the higher one shows less confinement within active region.

In Figure 4, the dispersion relation of the square of the momentum matrix elements for TE-polarization described at eqn. [5], have been shown for the designed laser system. The C1-HH1 and C1-LH1 transitions have strong TE components near the zone center. Since the compressive strain in the quantum well makes the top few valence subband HH- or LH-like, the dominant transitions for this structure are TE polarized.
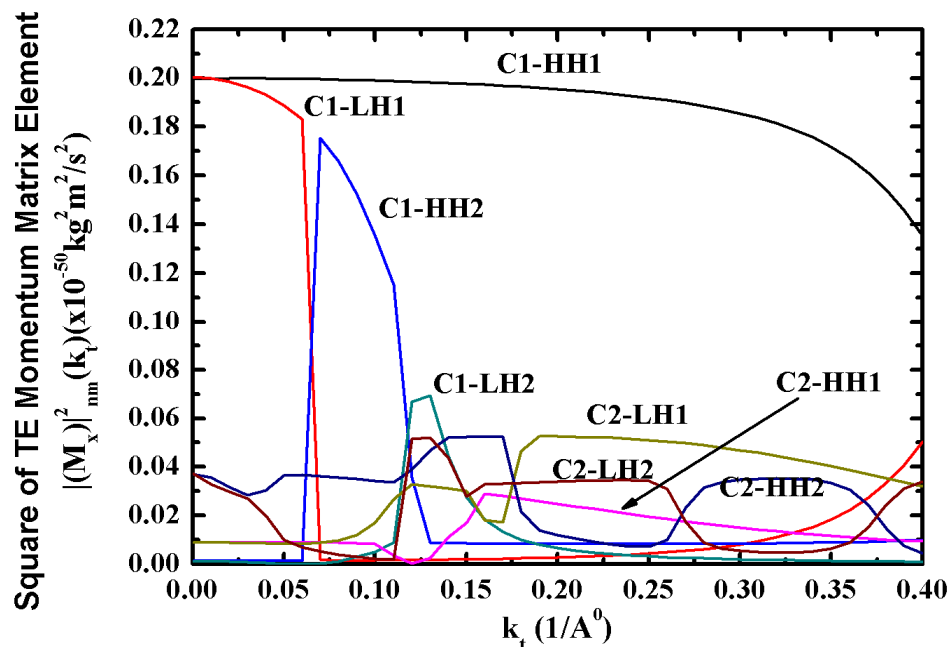

Figure 4. Square of momentum matrix elements of the TE-polarization for InN (12 Å) / In$_{0.25}$Ga$_{0.75}$N (15 Å) SQW at carrier density of 5×10^{19} cm^{-3}.
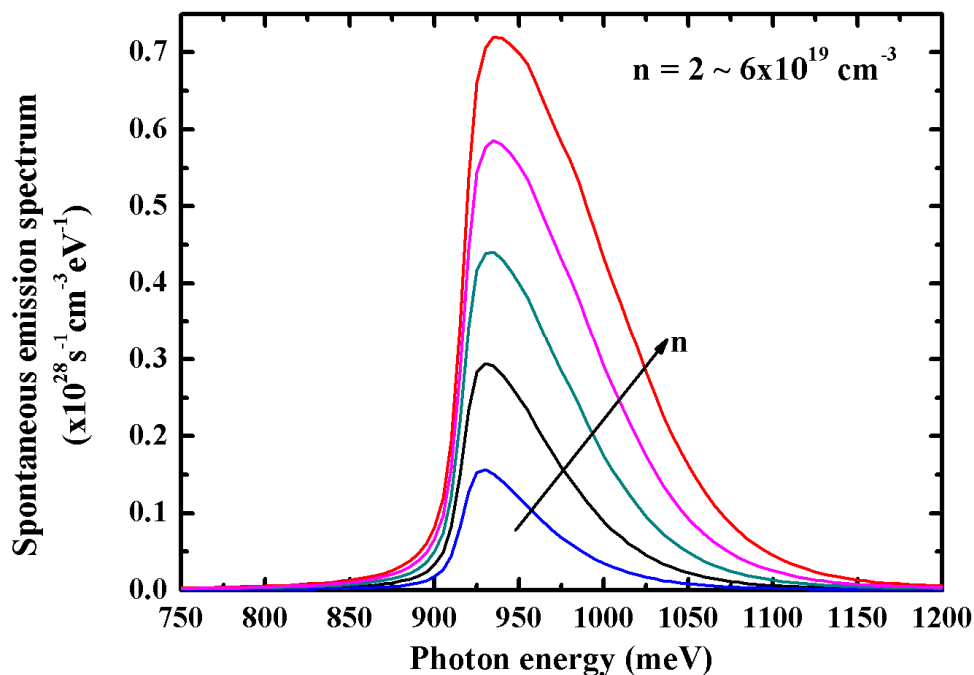

Figure 5. Spontaneous emission spectra of strained 12Å InN-In$_{0.25}$Ga$_{0.75}$N quantum well with GaN layer for carrier density (n) form 2×10^{19}cm^{-3} up to 6×10^{19}cm^{-3} at T = 300 K.

Following the equation [9], the spontaneous emission spectra for InN-In$_{0.25}$Ga$_{0.75}$N has been calculated using the simulation model and illustrated in Figure 5 for a range of carrier density of 2×10^{19}cm^{-3} up to 6×10^{19}cm^{-3} at T = 300 K. From the figure, it is seen that increase in carrier density increases the peak emission amplitude and shows a slight blue-shift of the peak emission wavelength. Spontaneous emission spectrum depends on the electron-hole wavefunction overlap factor. Higher overlap will cause higher spontaneous emission rate. From the calculation of the spontaneous emission rate, the material gain for the structure have been calculated for both TE and TM polarization. Material gain or optical gain of a laser means the growth of the optical signal per unit length. Optical gain of semiconductor laser is also described as the optical amplification in the semiconductor materials. In Figure 6, the optical gain of the Laser has been shown for a range of carrier density from 2×10^{19} cm^{-3} to 6×10^{19} cm^{-3}. Figure shows that the peak optical gain increases with the increase of the injection carrier density and the peak wavelength shows a blue shift which agrees with the previously published works (14).
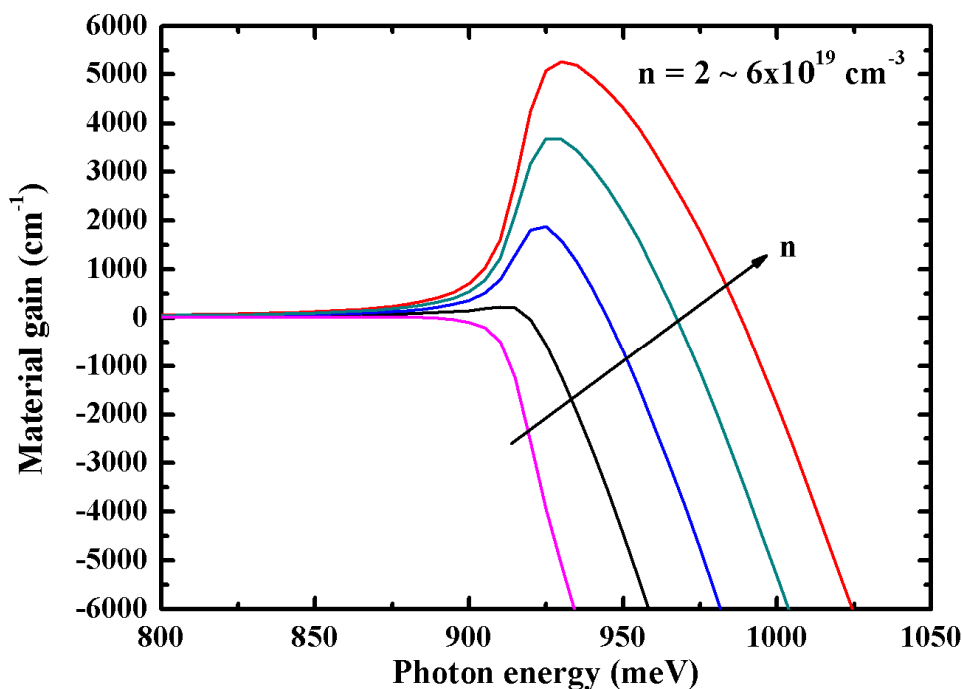

Figure 6. TE polarized optical gain spectra of strained 12Å InN - In$_{0.25}$Ga$_{0.75}$N quantum well with GaN layer for carrier density form 2×10^{19} cm^{-3} up to 6×10^{19} cm^{-3} at T = 300K.

Figure 7 illustrates the spontaneous emission radiation recombination rate per unit volume (R_{sp}) of 12Å InN-In$_{0.25}$Ga$_{0.75}$N quantum well structure plotted against carrier density (n) for low carrier density ($n = 2×10^{18}$ cm^{-3} up to 10×10^{18} cm^{-3}) and high carrier density ($n = 2×10^{19}$ cm^{-3} up to 6×10^{19} cm^{-3}) regimes respectively. Designed structure shows a significant improvement of the radiative recombination rate for the high carrier density regime where the threshold carrier density of QW structure exists. This enhancement indicates the application of the designed structure for laser operation with higher radiative efficiency. From the equation [10], it has been found that at radiative current density above 30 Acm^{-2}, the structure shows an increase in optical gain and with the increase in current density the optical gain increases significantly.
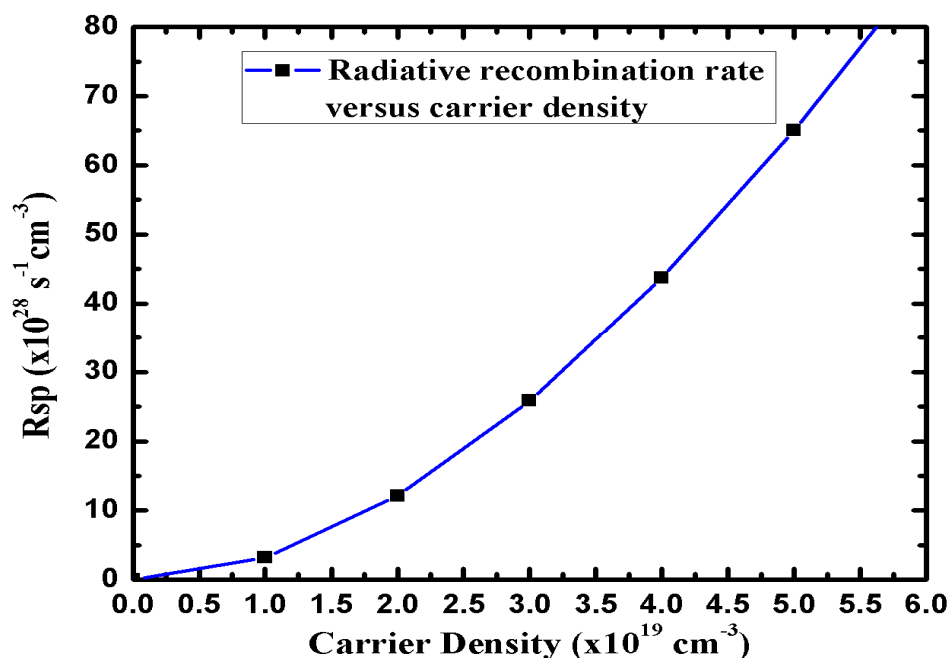
Figure 7. Spontaneous emission radiative recombination rate per unit volume as a function of carrier density at 300 K for 12Å InN-In$_{0.25}$Ga$_{0.75}$N quantum well.

Conclusion

In this work, a wurtzite nitride-based single quantum well laser has been designed and analyzed for attaining the wavelength of 1330nm. Here, 12Å InN layer has been used as well material along with 15Å In$_{0.25}$Ga$_{0.75}$N layer as barrier material and GaN as SCH layer. Several electrical and optical characteristics have been analyzed for the system. Optical transitions between conduction subbands and valence subbands for TE-polarization have been presented. Spontaneous emission rate and optical gain with a range of carrier densities have been performed for the structure. At higher carrier density, the peak of both spontaneous emission rate spectra and optical gain spectra shows a shift towards lower wavelength. The sweeping range of the carrier density is from 2×10^{19} cm^{-3} up to 6×10^{19} cm^{-3} at T = 300K. With the increase of carrier density, the peak amplitude of the calculated spontaneous emission and optical gain spectra shows an increase in amplitude. It has been found that, at 3×10^{19} cm^{-3} carrier density, the spontaneous emission spectrum gives peak amplitude of 2.946×10^{27} s^{-1}cm^{-3}eV^{-1} at 1336.7 nm and the peak optical gain of 222.587 cm^{-1} occurs at 1366.1 nm. At 6×10^{19} cm^{-3}, the peak amplitude of spontaneous emission spectrum of 7.21×10^{27} s^{-1}cm^{-3}eV^{-1} occurs at 1329.55 nm and the peak optical gain of 5261.52 cm^{-1} occurs at 1336.7 nm.

Acknowledgements

References

1. D.F. Feezell, M.C. Schmidt, R.M. Farrell, K.C. Kim, M. Saito, K. Fujito, D.A. Cohen, J.S. Speck, S.P. DenBaars and S. Nakamura, *Jpn. J. Appl. Phys.*, **46**, L284 (2007).

2. K. Iso, H. Yamada, H. Hirasawa, N. Fellows, M. Saito, K. Fujito, S.P. DenBaars, J.S. Speck and S. Nakamura, *Jpn. J. Appl. Phys.*, **46**, L960 (2007).

3. Y. K. Ee, J. M. Biser, W. J. Cao, H. M. Chan, R. P. Vinci, and N. Tansu, *IEEE J. Sel. Topics Quantum Electron*, **15**(4), 1066 (2009).

4. J. Zhang, J. Yang, G. Simin, M. Shatalov, M.A. Khan, M.S. Shur and R. Gaska, *Appl. Phys. Lett.*, **77**, 2668 (2000).

5. I. Vurgftman and J.R. Meyer, *J. Appl. Phys.*, **94(**6), 3675 (2003).

6. H.J.R. Dutton, *Understanding Optical Communications*, IBM (1998).

7. J. Hayes, *The Fiber Optic Association (FOA) – Tech Topics*.

8. H. Machhadani, P. Kandaswamy, S. Sakr, A. Vardi, A. Wirtmuller, L. Nevou, F. Guillot, G. Pozzovivo, M. Tchernycheva, A. Lupu, L. Vivien, P. Crozat, E. Warde, C. Bougerol, S. Schacham, G. Strasser, G. Bahir, E. Monroy and F.H. Julien, *New J. Phys.*, **11**, 120523 (2009).

9. H. Zhao, G. Liu and N. Tansu, *Appl. Phys. Lett.*, **97**, 131114 (2010).

10. J. Hecht, *McGraw-Hill Comp. Inc.*, New York (1993).

11. S.L. Chuang, *IEEE J. Quantum Electronics*, **32(**10), 1791 (1996).

12. J. Bardeen and W. Shockley, *Phys. Rev.*, **80**, 72 (1950).

13. F. Bernardini and V. Fiorentini, *Phys. Stat. Sol. (b)*, **216**, 391 (1999).

14. H. Zhao, R.A. Arif, Y.K. Ee and N. Tansu, *IEEE J. Quantum Electronics*, **45(**1), 66 (2009).

15. J. Piprek, *Nitride Semiconductor Devices: Principles and Simulation*, p. 24, Wiley-VCH, New Jersey (2007).

16. W.W. Chow and M. Kneissl, *J. Appl. Phys.*, **98**, 114502 (2005).